Received: 1 September 2023 | Revised: 5 January 2024 | Accepted: 6 January 2024

DOI: 10.1002/mrm.30023

RESEARCH ARTICLE

Magnetic Resonance in Medicine

In vivo monitoring of renal tubule volume fraction using dynamic parametric MRI

Ehsan Tasbihi[1,2] | **Thomas Gladytz**[1] | **Jason M. Millward**[1,3] | **João S. Periquito**[1] | **Ludger Starke**[1,4] | **Sonia Waiczies**[1,3] | **Kathleen Cantow**[5] | **Erdmann Seeliger**[5] | **Thoralf Niendorf**[1,4]

[1]Berlin Ultrahigh Field Facility, Max Delbrueck Center for Molecular Medicine in the Helmholtz Association, Berlin, Germany

[2]Charité–Universitätsmedizin Berlin, Berlin, Germany

[3]Hasso Plattner Institute for Digital Engineering, University of Potsdam, Potsdam, Germany

[4]Experimental and Clinical Research Center, a Joint Cooperation Between the Charité Medical Faculty and the Max Delbrück Center for Molecular Medicine, Berlin, Germany

[5]Institute of Translational Physiology, Charité–Universitätsmedizin Berlin, Berlin, Germany

Correspondence
Thoralf Niendorf, Max Delbrück Center for Molecular Medicine in the Helmholtz Association, Robert Rössle Strasse 10, 13125 Berlin, Germany.
Email: thoralf.niendorf@mdc-berlin.de

Funding information
German Research Foundation, Grant/Award Numbers: SFB 1365, (394046635)

Abstract

Purpose: The increasing incidence of kidney diseases is a global concern, and current biomarkers and treatments are inadequate. Changes in renal tubule luminal volume fraction (TVF) serve as a rapid biomarker for kidney disease and improve understanding of renal (patho)physiology. This study uses the amplitude of the long T_2 component as a surrogate for TVF in rats, by applying multiexponential analysis of the T_2-driven signal decay to examine micromorphological changes in renal tissue.

Methods: Simulations were conducted to identify a low mean absolute error (MAE) protocol and an accelerated protocol customized for the in vivo study of T_2 mapping of the rat kidney at 9.4 T. We then validated our bi-exponential approach in a phantom mimicking the relaxation properties of renal tissue. This was followed by a proof-of-principle demonstration using in vivo data obtained during a transient increase of renal pelvis and tubular pressure.

Results: Using the low MAE protocol, our approach achieved an accuracy of MAE $< 1\%$ on the mechanical phantom. The T_2 mapping protocol customized for in vivo study achieved an accuracy of MAE $< 3\%$. Transiently increasing pressure in the renal pelvis and tubules led to significant changes in TVF in renal compartments: $\Delta TVF_{cortex} = 4.9\%$, $\Delta TVF_{outer\_medulla} = 4.5\%$, and $\Delta TVF_{inner\_medulla} = -14.6\%$.

Conclusion: These results demonstrate that our approach is promising for research into quantitative assessment of renal TVF in in vivo applications. Ultimately, these investigations have the potential to help reveal mechanism in acute renal injury that may lead to chronic kidney disease, which will support research into renal disorders.

KEYWORDS

kidney, MRI, multi-exponential analysis, T_2 mapping, tubule volume fraction

1 | INTRODUCTION

The kidney is a remarkable organ, eliminating water-soluble waste products and maintaining the body's osmolyte and water balance. The nephron is the functional unit of the kidney for urine formation and for maintaining these balances; it consists of the glomerulus and the tubule. In the renal cortex, the glomerulus produces primary urine by ultrafiltration of blood plasma. The tubule reabsorbs most of the filtered water and osmolytes, and secretes some substances, to produce the final urine. The tubule consists of highly differentiated segments: The proximal tubule, located in the cortex, is followed by the U-shaped loop of Henle, which dips into the medulla, then returns to the cortex. This is followed by the distal tubule, and finally the collecting duct, running from the cortex through the medulla, ending at the renal papilla where the final urine drains into the extrarenal urinary tract.

The volume of the tubular lumen accounts for a large fraction of the kidney volume.[1,2] This tubular volume fraction (TVF) can change due to changes in (i) glomerular filtration rate (GFR), (ii) tubular water reabsorption, (iii) transmural pressure of the tubules, and (iv) outflow of final urine into the extrarenal urinary tract. Pathophysiologically relevant decreases in the TVF can result from primary decreases in GFR due to reduced effective filtration pressure in clinical scenarios including circulatory shock, low arterial target pressure during cardiopulmonary bypass, and surgery involving clamping of the suprarenal aorta or the renal artery. Other causes for decreased TVF include decreased hydraulic conductance of the filter, which occurs in some forms of glomerulonephritis, and diffuse tissue fibrosis.[3–8] Increases in TVF due to primary GFR increase are typical for the early stages of diabetic kidney disease.[9] TVF also increases in scenarios with reduced water reabsorption, such as following therapeutic administration of diuretics (particularly osmotic and loop diuretics), and due to hyperglycemia.[10] Increased tubular pressure resulting from increased tubular fluid viscosity following administration of X-ray contrast media during transcutaneous cardiac procedures also increases TVF.[11,12] Another cause for increased TVF is obstruction of the extrarenal urinary tract: the renal calices, pelvis, ureter, bladder, and the urethra. Such congestions can be caused by kidney stones, tumors, scar tissue, and hyperplasia of the prostate, and can also occur during endourologic procedures.[13–16] Polycystic kidney disease is also characterized by progressive increase in the TVF.

Parametric mapping of T_2 is an established MRI approach. The water-containing compartments of renal tissue include the (i) intracellular space, (ii) interstitial space, (iii) lumen of the intrarenal vasculature with flowing blood, and (iv) tubular lumen with flowing tubular fluid—a compartment unique to the kidney. For parametric mapping, the T_2 relaxation decay is quantified voxel-wise. Because most renal MRI studies use a voxel size that includes at least two, but usually all four fluid compartments, the T_2 signal decay curve must be multiexponential, with multiple T_2 relaxation times, to account for partial volume effects.[17–19] Because the parenchyma and blood compartments exhibit a similar T_2, and only the tubular fluid has a considerably longer T_2 relaxation, the T_2 decay curves can be approximated with a bi-exponential decay. Zhao et al. reported a T_2 of approximately 41 ms for the renal cortex and T_2 of approximately 52 ms for the outer medulla[20,21]; for arterial blood, a T_2 of about 40 ms was reported by Lee et al.[22] If the T_2 decay is sampled at appropriate time points, the contributions of slow and fast T_2 relaxation components can be separated with bi-exponential modeling to provide useful information on the renal microstructure.[23,24]

This study aims to evaluate T_2 mapping as a tool to noninvasively probe renal tissue properties in vivo as a potential marker for early diagnosis of kidney diseases. In this work, we define TVF as the internal volume of the tubular lumen that varies with changes in the tubular fluid volume, not the total volume that includes the tubular epithelial cells. We developed a protocol for T_2 mapping of the rat kidney and determined a numerical solution for multi-exponential decomposition of the T_2 decay. We evaluated and validated the protocol and algorithms using synthetic data, followed by MRI measurements, in a purpose-built multicompartment test phantom to determine the accuracy of our method for T_2 mapping protocols for which the ideal range of T_2 weighting is not known a priori.[25] We then applied our quantitative analysis approach to in vivo data acquired in rats that underwent a clinically relevant intervention—a short-term increase in pelvis and tubule pressure (TPI)—that induces changes in kidney size and T_2.[23] This allowed us to derive TVF maps of the rat kidney, to investigate the relationship between tubule pressure and TVF, and asses the feasibility of our approach to detect clinically meaningful changes in TVF.

2 | METHODS

2.1 | Decomposition of the T_2 decay to obtain tubule water fraction

The T_2 time of water is determined by its local environment.[24,26,27] Accordingly, tubular fluid, originating from ultrafiltration in the glomeruli, has a substantially longer T_2 relaxation time compared with the renal parenchyma and blood. Hence, the tubule luminal water contribution

to the MR signal should be separable from the tissue and blood signal using nonlinear least squares regression. Each voxel (typically $0.25 \times 0.25 \times 1$ mm, preclinical)[24,25] provides a T_2 decay that consists of a long T_2 component related to tubular fluid and short T_2 components related to parenchyma and blood. These components can be separated using a two-order exponential decay as follows:

$$I(t) = A_1^* \exp\left(-t/T_{2\_long}\right) + A_2^* \exp\left(-t/T_{2\_short}\right) \quad (1)$$

where I(t) is the signal amplitude; t is the evolution time used for T_2 weighting; T_{2_long} and T_{2_short} are the T_2 relaxation times of the long and short components; and A_1 and A_2 are the initial signal amplitudes of the long and short components. Typical values of T_2 for the renal tissue layers of healthy rats at 9.4 T are 90.0–68.5 ms in the inner medulla (IM), 50.0–43.0 ms in the outer medulla (OM), and 43.0–36.6 ms in the cortex (CO).[20,21] Therefore, we considered a relaxation time range of 10–100 ms for T_{2_short} to represent renal parenchyma and blood. To determine the T_{2_long} component of rat kidney, we measured the T_2 of pure water using our 9.4T scanner. An average T_2 of 500 ms was found to represent pure water at body temperature of 37ºC. A T_{2_long} of about 500 ± 70 ms was found for the renal cortex of healthy rats using a free bi-exponential fit. Assuming that substances normally present in the tubular fluid of healthy subjects do not significantly affect T_{2_long}, the T_{2_long} of tubular fluid should remain constant across kidney layers.[28] Therefore, we considered 500 ms to be an appropriate approximation for the T_2 relaxation time of tubular fluid, which was fixed in the bi-exponential fitting.

We applied double exponential models along with Trust-Region optimization from *MATLAB* (The MathWorks, Natick, MA, USA) functions to estimate the parameters for the bi-exponential models. Trust-Region methods are highly effective and considered the gold standard in various applications.[29–31] Instead of fitting three or more exponentials, we used a bi-exponential model. The advantage of a bi-exponential model is to simplify the multi-exponential model and improve the accuracy of the resulting T_2 and amplitudes. A three-exponential model will not correctly differentiate parenchyma and blood as two different compartments when their respective T_2 values are too similar and overlap.

Accuracy of T_2 mapping and fitting in in vivo studies is limited by the constraints of acquisition time, spatial resolution, and SNR. To address this, we applied bi-exponential decomposition of simulated T_2 mapping data covering a range of SNR and T_2 conditions. From these simulations we determined a low mean absolute error (MAE) protocol and an accelerated protocol customized for the in vivo study for T_2 mapping of the rat kidney at 9.4 T.

2.2 | Evaluation using synthetic data and simulations of T_2 decay data

To generate synthetic data for simulations, we defined a model consisting of two components: a long T_2 component related to tubular fluid and a short T_2 component related to renal parenchyma and renal blood. We developed a two-compartment-model for a multi-echo spin-echo signal decay using a Bloch-simulation toolkit (http://www-mrsrl.stanford.edu/~brian/blochsim/). This toolkit provides the magnetization vector at each given time after the initial excitation and for each image voxel based on the extended phase graph (EPG) formalism.[32,33] This approach was used to estimate the actual T_2 echo modulation curve in a realistic multi-echo spin-echo experiment using non-ideal refocusing pulses.[34,35] The simulated T_2 decay could be composed as follows:

$$S(t) = M_0 \sum_{j=1}^{2} \left(D_j(T_2).\mathrm{EPG}(T_2\theta) dT_2 + \varepsilon(0, \sigma n) \right) \quad (2)$$

where S(t) is the signal amplitude; M_0 represents the initial magnetization and signal intensity TE = 0, which is equal to the assumed proton density, and $j = 2$, the number of water compartments; D_j denotes the amplitude associated with each compartment, and j is the compartment index; θ^- denotes all other required parameters. The $\varepsilon(0, \sigma n)$ function indicates the additive white Gaussian noise. Gaussian-distributed white noise was applied to the signal, such that SNR = mean(s)/σ is similar to the noise typically found in the magnitude images from in vivo studies. A dictionary of simulated T_2 decay curves was acquired by repeating the simulations with different T_{2_short} = [5, 10, 15, 20, 25, 30, 35, 40, 45, 50, 60, 70, 85, 100 ms], T_{2_long} = 500 ms, T_{1_short} = 1820 ms, T_{1_long} = 3400 ms, refocusing flip angle = (122°–180°, 2° increments), echo spacing = [5, 6, 7, 8, 9, 10, 12, 13, 15, 16, 18, 20, 22, 24, 26, 28, 30, 32, 34, 36, 38, 41, 44, 47, 50 ms], SNR = [5, 10, 20, 30, 50, 80, 120, 180, 270, 400, 600], and TVF = 0%–95% (5% increments).

2.3 | Validation in a phantom study

To evaluate the accuracy of the bi-exponential decomposition, we developed a mechanical phantom that emulates a two-compartment system. This phantom mimics the T_2 relaxation properties of renal tissue but does not mimic the microstructure of renal tubules and parenchyma. Figure 1 shows a photo and schematic of the custom-built phantom. The housing was designed and printed with cylindrical geometry (D = 50 mm) using *Fusion 360* (Autodesk, Inc., San Francisco, CA, USA) and a 3D printer

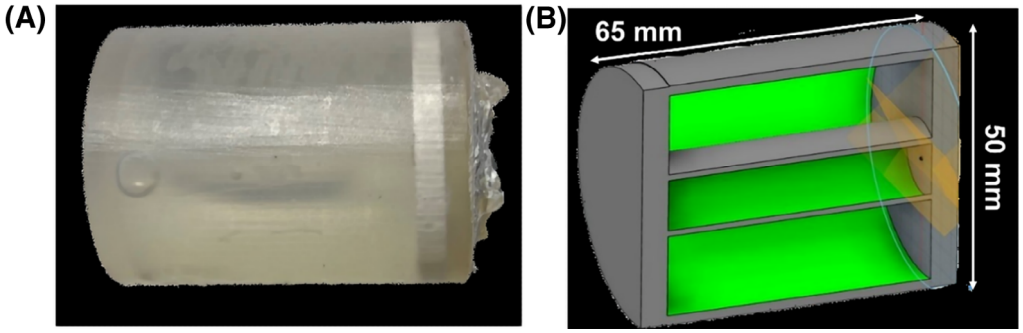

FIGURE 1 A, Photograph of the mechanical phantom. B, Schematic view of the phantom. The middle tube was filled with doped water with T_2 mimicking renal T_2 and surrounded by distilled deionized water. This is simple and easy to make, and it is possible to define circular regions of interest in the center, with different diameters, to examine water percentage changes. The dimensions of the housing for the phantom (outer diameter = 50 mm, inner diameter = 10 mm, length = 65 mm) were adjusted to the size of the magnet bore; the material used was magnetically compatible.

(Dimension 1200es; Stratasys Ltd., Rehovot, Israel). The phantom includes distilled de-ionized water and water doped with a mixture of $MnCl_2$ and $CuSO_4$ to achieve T_2 and T_1 relaxation times that mimic the T_1 and T_2 of renal parenchyma[21,36] and can be used to simulate relative changes of the tubule water fraction within the expected ranges.[37]

2.4 | Proof-of-principle in vivo study

All experiments were approved by the Animal Welfare Department of the State Office of Health and Social Affairs of Berlin, in accordance with German Animal Protection Law and approved guidelines. Male Wistar rats ($n = 7$, aged 12–13 weeks, mass 270–300 g; Harlan-Winkelmann, Borchen, Germany) were used. The animals had ad libitum access to standard diet and water and were housed under standard conditions with environmental enrichment.[23,38]

Rats underwent surgical procedures involving insertion of vascular catheters and invasive probes for quantitative measurements of renal hemodynamics and oxygenation, as previously described.[23] For anesthesia, urethane (0.2 g/mL in distilled water; 6 mL/kg bodymass intraperitoneal; Sigma-Aldrich, Steinheim, Germany) was used throughout the surgical preparation and examination.[23,39–42] The surgical preparation included insertion of a catheter in the left ureter with its tip in the renal pelvis.[23] The catheter was connected to a saline-filled container placed outside of the MR scanner, which was elevated 41 cm above the kidney of the rat to remotely increase the pressure in the ureter, renal pelvis, and the tubules by about 30 mm Hg (Figure 2). This experimental intervention is clinically relevant, as upper urinary tract endourologic procedures often cause temporary increases in tubular and intrarenal pressure.[16,23,43] Effectiveness of the TPI intervention was monitored by changes in near-infrared transmission through the kidney.

The animals were transferred from the adjacent surgery lab to the MR scanner using an in-house-designed animal holder adapted to the geometry of the MR scanner, allowing the ureteral catheter to stay fixed in position.[39,44,45] During scanning, body temperature was maintained at 37°C with circulating warm water (Thermo Haake GmbH, Karlsruhe, Germany), monitored with a rectal probe (AccuSens; Opsens, Québec City, Canada). Respiration rate was monitored using a balloon placed on the chest (Model 1025; SA Instruments, Stony Brook, NJ, USA), which also served for triggering the MRI acquisition.

MRI data were acquired on a 9.4T small animal MR system (Bruker Biospec 94/20; Bruker Biospin, Ettlingen, Germany) using a linear RF volume resonator and a four-channel surface RF coil array tailored for rats (Bruker Biospin).[23] For geometric planning and slice positioning, T_2-weighted pilot scans were acquired. Local volume-selective shimming of the magnetic field homogeneity on a voxel accommodating the left kidney was conducted using an automatic optimization algorithm based on FID length. T_2 mapping was performed with respiratory-gated imaging protocols.[23] For T_2 mapping, a multi-echo spin-echo technique (TR ~ 500 ms depending on respiration gating, number of echoes = 13, first TE = 6.4 ms, interecho time ΔTE = 6.4 ms, number of averages = 1, $\alpha_{\text{refocusing pulse}} = 180°$, $t_{\text{acquisition}} = 58$ s) was used. For T_2 mapping, a midcoronal oblique image slice was acquired using in-plane spatial resolution = 226 × 445 μm^2, FOV = 38.2 × 50.3 mm^2, matrix size = 169 × 113 (zero-filled to 169 × 215), and slice thickness = 1.4 mm.

The workflow was as follows: control baseline period of about 10 min; short-term increase of renal pelvis and

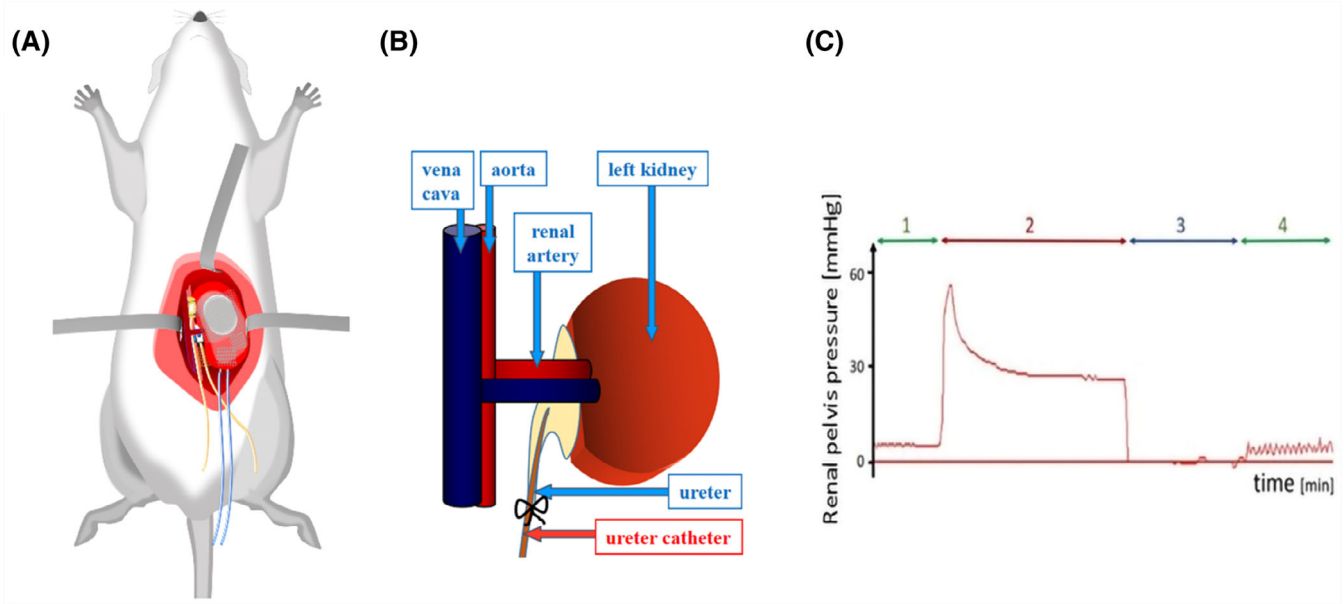

FIGURE 2 Illustration of the methods used for remotely controlled brief increases in renal pelvis and tubular pressures. A, Schematic view depicting the relevant positions and fixations of probes. B, Catheter placed in the left ureter and connected via a catheter (length ~ 1.5 m) to a container filled with isotonic saline. Elevating the container 41 cm above the level of the rats' kidneys increased pelvis and tubular pressures by about 30 mm Hg. C, Pressure trace obtained for the renal pelvis of a rat (pressure transducer: DT-XX; Viggo-Spectramed, Swindon, UK; amplifier & acquisition: TAM-A Plugsys & HAEMODYN; Hugo Sachs Elektronik, March, Germany) recorded during baseline control conditions (1, *green*), during pressure increase achieved by injection of saline fluid via the ureteral catheter (2, *red*), following disconnection of the catheter to obtain zero pressure for calibration of the pressure measurement (3, *dark blue*), and during another control measurement (4, *green*). Note that the oscillations observed during control (1) and, even enlarged, during control (4) represent the spontaneous peristaltic contractions of the ureter.

tubular pressure (average duration 10 ± 2 min, depending on respiratory gating); and follow-up recovery phase of 10 min. The first subgroup of rats ($n = 3$) underwent two baseline T_2 mapping MR scans before TPI, one T_2 mapping scan during the TPI intervention, and one T_2 mapping scan during the recovery phase. In the second subgroup ($n = 4$), the rats underwent three T_2 mapping scans during the baseline period, four scans during the TPI intervention, and one T_2 mapping scan during the recovery phase.[23]

Data from these in vivo experiments were used for kidney-size determination by MRI in pathophysiological settings.[23] In the current study, we used data from these experiments for a new purpose, to assess the feasibility of our method in detecting relative changes in the TVF. This approach allows us to enhance the value and impact of in vivo studies in experimental animals, aligning with the ethical principles of the 3Rs for animal research.

2.5 | Image analysis and statistics

Parametric maps of absolute T_2 were calculated by pixel-wise mono-exponential fitting to the signal intensities of the T_2-weighted images acquired at different TEs.[23] Median T_2 values for regions of interest (ROIs) within CO, OM, and IM were calculated from the T_2-weighted images acquired at different TEs.[46,47] TVF maps were extracted using pixel-wise bi-exponential fitting to the signal intensities of the T_2-weighted images acquired at different TEs. For the fitting procedure, T_2 was fixed to 500 ms for tubular water. For parenchyma and blood, the integration limit was set to $T_2 = 10$–100 ms.

To compute the tubule water fraction, the ratio of the weight of longer T_2 to the total sum of weights was determined as follows:

$$TVF = \frac{A(T_{2\_long})}{A(T_{2\_short}) + A(T_{2\_long})} \tag{3}$$

where $A(T_{2\_long})$ is the weight corresponding to the tubule water component, and $A(T_{2\_short})$ is the weight corresponding to renal parenchyma and blood.

For synthetic data simulations, the MAE was used to show the percentage difference between the calculated value and the true value using, as follows:

$$\mathrm{MAE} = \frac{\sum_{n=1}^{N} | x' - x |}{\mathrm{N}} \tag{4}$$

where x is the ground truth; x' is the estimated result of the *n*th trial; and N denotes the number of trials ($N = 1000$). SNR levels ranging from 5 to 600 were investigated. To determine the impact of errors in the transmission-field B_1^+ on TVF estimation, refocusing flip angles ranging from 122° to 180° were investigated.

After applying the bi-exponential analysis, from Eq. (1), the TVF was determined by applying T_1 correction. The overall signal intensity (S) of a spin-echo pulse sequence can be approximated as follows:

$$S = K.[H].\left(1 - e^{-\frac{TR}{T1}}\right).\left(e^{-\frac{TE}{T2}}\right) \quad (5)$$

where [H] is the proton density and K is a scaling factor. Considering the individual terms, it is apparent that T_1 effects are connected to the TR; T_2 effects are connected to the TE; and [H] effects are always present. When TR is long compared with T_1, the T_1-weighting term $e^{-TR/T1}$ approaches 0, so that T_1 effects are largely reduced or absent and can be neglected. For protocols in which TR is not long enough to ensure full T_1 relaxation, T_1 saturation effects occur and might compromise the TVF assessment because both compartments may present a different degree of T_1 weighting. Considering the overall signal intensity (S) for a bi-exponential model,

$$S = S_{long} + S_{short} \quad (6)$$

T_1 effects were corrected by dividing the signal intensity for each compartment by $(1\text{-}e^{-TR/T1})$ as follows:

$$\begin{aligned} S_{long\_corrected} &= S_{long}/\left(1 - (\exp[-TR/T1_{\_long}]\right); \\ S_{short\_corrected} &= S_{short}/\left(1 - (\exp[-TR/T1_{\_short}]\right) \end{aligned} \quad (7)$$

TR is determined individually in every scan according to the respiration rate. Values of $T_{1\_long} = 3400$ and $T_{1\_short} = 1820$ ms are T_1 relaxation times in renal parenchyma, blood, and pure water at 37°C acquired from literature and own measurements.[20]

Data from the in vivo experiments were evaluated for Gaussian distribution using the Shapiro–Wilk test. Given the different numbers of scans between the first and second subgroups, the mean TVF was calculated for the baseline and intervention phases, and this was used for the analysis. Changes in TVF in response to the TPI intervention were analyzed using the nonparametric repeated-measures Friedman test, followed by Dunn's post hoc test with the Benjamini-Hochberg correction for multiple comparisons. Data were analyzed and visualized using Rv.3.6.3 with the packages "rstatix," "dunn. Test," and "rayshader."[48–50] p-Value < 0.05 was considered significant.

3 | RESULTS

3.1 | Evaluation with synthetic data and simulations

We simulated T_2 decay curves to examine the accuracy of our T_2 fitting procedure and to investigate the effect of imaging protocol parameters on the TVF assessment. Figure 3 shows a representative example of synthetic data simulating T_2 echo curves for a two-component model, in which the contribution of the fast component varies from 1% to 95%. Figure 4A provides an overview of the impact on TVF estimation of varying the interecho spacing ΔTE from 5 to 50 ms and SNR from 5 to 600. The parameters were set to $T_{2\_short} = 50$ ms, $T_{2\_long} = 500$ ms, number of echoes = 13, $\alpha_{refocusing\ pulse} = 180°$, to be consistent with the T_2 protocol used for our in vivo experiments, designed to balance the constraints of acquisition time, spatial resolution, and SNR. MAE decreased with increasing SNR and increasing echo spacing. With a realistic SNR = 30 and ΔTE = 15 ms, the average error of 1000 trials was estimated to be 2.1%. Increasing the echo spacing to ΔTE ≥ 50 ms did not further reduce the MAE. For the smallest ΔTE = 5 ms and SNR = 30, an MAE = 11.2% was observed. This is because at a fixed number of echoes and a short TE, only a smaller segment of the decay is covered so that the long component is not primarily considered. For ΔTE = 6.4 ms (in vivo protocol), a MAE = 8.5% was found. For a very low SNR ≤5, a MAE >10% was obtained.

To assess the impact of flip angle on TVF estimation, refocusing flip angles ranging from 122º to 180° and SNR = 5–600 were used (Figure 4B). MAE increased

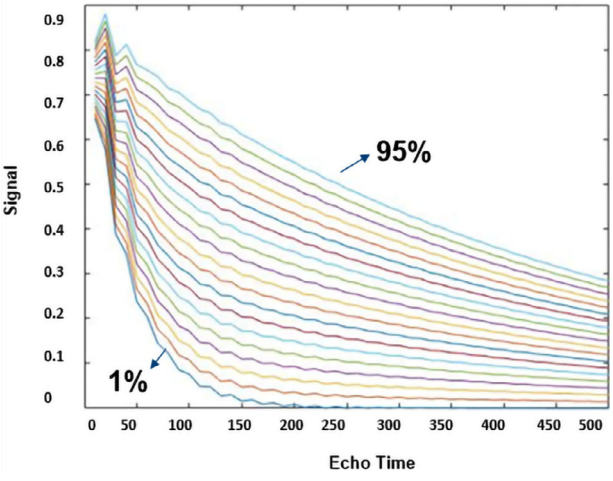

FIGURE 3 Representative example of synthetic data simulating T_2 echo decay curves for a multi-component model, in which the contribution of the fast component varies from 1% to 95%. Oscillations in every signal decay are due to imperfect refocusing pulses (here, 142°).

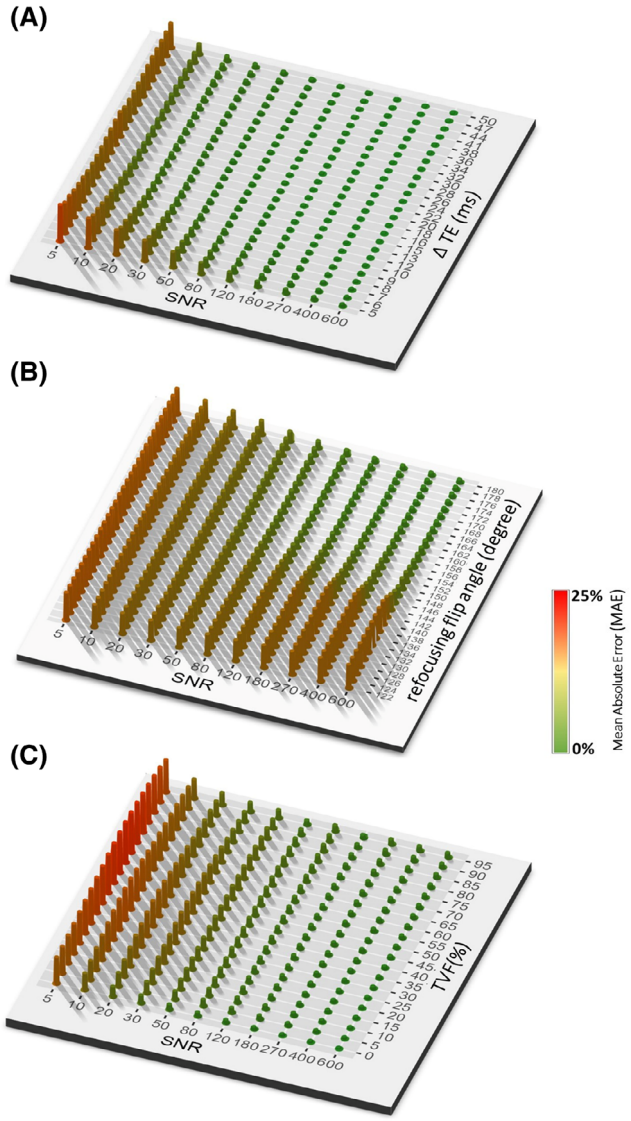

FIGURE 4 Representative examples of mean absolute error (MAE) calculated after analyzing the T_2 decay of the synthetic data with bi-exponential analysis. A, Effect of SNR and the interecho spacing on the accuracy of tubular volume fraction (TVF) estimation. Other simulation parameters were $T_{2\_long} = 500$ ms, $T_{2\_short} = 50$ ms, number of echoes = 13, $\alpha_{\text{refocusing pulse}} = 180°$. B, Effect of SNR and the refocusing flip angle on TVF estimation. Other simulation parameters were $T_{2\_long} = 500$ ms, $T_{2\_short} = 50$ ms, number of echoes = 13, and interecho time $\Delta TE = 6.4$ ms. C, Impact of changes in the TVF contributions to the signal intensity and SNR on TVF estimation. Other simulation parameters were $T_{2\_long} = 500$ ms, $T_{2\_short} = 50$ ms, number of echoes = 13, interecho time $\Delta TE = 6.4$ ms, and $\alpha_{\text{refocusing pulse}} = 180°$.

with decreasing SNR and decreasing refocusing flip angle. With a SNR = 30 and $\alpha = 164°$, the average MAE was estimated to be 8.6%. Figure 4B shows that for a realistic SNR = 30, the MAE for $\alpha = 150°–180°$ increased by only about 2% at smaller refocusing flip angles, in the range $\alpha = 122°–150°$. At higher SNR, the increase in MAE due to smaller refocusing flip angles was even more pronounced, indicating that α has a greater impact at higher SNR.

Next, we investigated the impact of changes in the TVF contributions to the signal intensity and SNR of the simulation parameters. Figure 4C summarizes the effect of the water fraction on TVF estimation for TVF = 0–0.95 and SNR = 5–600. For the protocol used for the in vivo experiments (SNR = 30, ΔTE = 6.4 ms, and a water fraction of 15%), the MAE was estimated to be 8.5%.

Table 1 summarizes the impact of a wrong fixation of T_{2_long} value during the fitting process on TVF assessment using synthetic data. The results show that misestimating of T_{2_long} may have an effect on the estimated TVF but does not considerably affect the relative changes (Δ).

3.2 | Validation in phantom study

After assessment of the synthetic data, we validated our bi-exponential approach in a phantom mimicking the relaxation properties of renal tissue. Before undertaking preclinical MRI investigations, appropriate MRI protocols should be carefully chosen to balance the competing demands of image quality, spatial resolution, and temporal resolution needed for the monitoring of the increase in the pelvis and tubular pressure. Based on our simulations, we chose two protocols: "low MAE protocol" (MAE = 2.4%) with parameters in a realistic range (TR = 4 s, number of echoes = 13, first TE = 15 ms, interecho time ΔTE = 15 ms, number of averages = 3, $t_{\text{acquisition}} = 47$ min, $\alpha_{\text{refocusing pulse}} = 180°$) and the accelerated protocol adapted for the in vivo measurements ("in vivo protocol"; TR = 500 ms, number of echoes = 13, first TE = 6.4 ms, ΔTE = 6.4 ms, number of averages = 1, $t_{\text{acquisition}} = 58$ s, $\alpha_{\text{refocusing pulse}} = 180°$) Figure 5A shows a T_2 map obtained for the phantom. The histogram (Figure 5B) shows the T_2 distribution for the selected ROI. Changes in the ratio of the volume fraction of the two compartments were achieved by changing the ROI size. Figure 5C shows TVF measured for the low-MAE protocol and for the accelerated protocol used in our in vivo study. For the low-MAE protocol, MAE < 1% was achieved in the phantom. For this in vivo protocol, an accuracy of 97.8% (MAE < 3%) was observed.

3.3 | In vivo study

After validating our approach in a phantom, we applied the TVF analysis to data acquired from an in vivo MRI study in healthy rats, as a proof-of-principle demonstrating the in vivo feasibility and sensitivity of our approach. We hypothesized that an increase in the pelvis and tubular

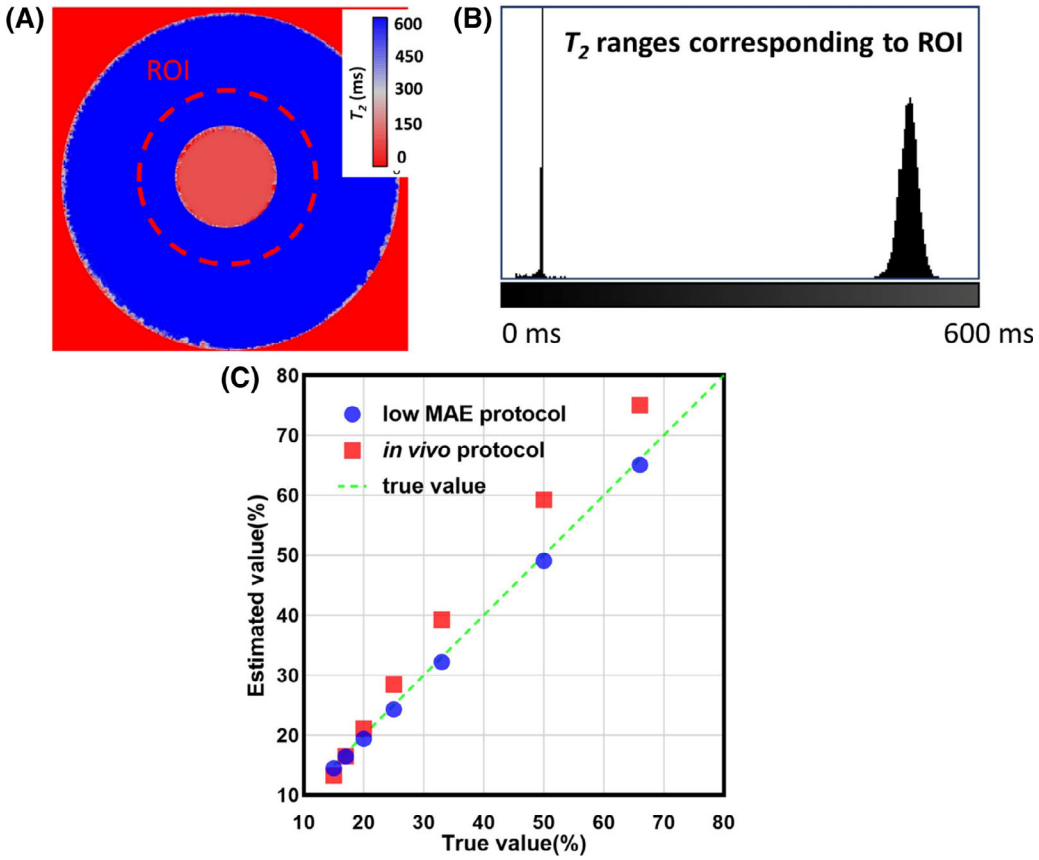

FIGURE 5 A, Reconstructed T_2 map in milliseconds of the custom-built T_1, T_2 phantom (scan parameters: T_2 [multi-echo spin echo], 13 echoes, echo spacing = 6.4 ms, TR = 500 ms). B, Exemplary region-of-interest (ROI) selection and histogram showing T_2 distribution corresponding to the selected ROI. C, Evaluation of the assessment of the volume fraction with decomposition of parametric T_2 in a mechanical phantom using the low–mean absolute error protocol derived from the simulations (true value; TR = 4 s, number of echoes = 13, first TE = 15 ms, interecho time ΔTE = 15 ms, $t_{acquisition}$ = 47 min, $\alpha_{refocusing\ pulse}$ = 180°, number of averages = 3) and the protocol adapted for the in vivo measurements (estimated value; TR = 500 ms, number of echoes = 13, first TE = 6.4 ms, interecho time ΔTE = 6.4 ms, number of averages = 1, $\alpha_{refocusing\ pulse}$ = 180°, $t_{acquisition}$ = 58 s). The correlation coefficient between the estimated and the true value is 0.997.

pressure would increase the TVF. Figure 6 shows representative renal T_2 maps obtained from a mono-exponential fit for seven rats in vivo during baseline, following intervention and recovery. After TPI, T_2 changes were readily apparent. Under baseline control conditions, T_2 relaxation times were $T_2 = 44 \pm 3.6$ ms (mean ± SD, $n = 7$ rats) for the CO; $T_2 = 54 \pm 5.2$ ms for the OM; and $T_2 = 88 \pm 16$ ms for the IM. During the TPI intervention, a prolongation of T_2 was detected for the CO ($T_2 = 49 \pm 4.3$ ms) and the OM ($T_2 = 57 \pm 6.3$ ms), and a T_2 shortening was observed for the IM ($T_2 = 63 \pm 11.4$ ms). Following termination of the TPI intervention, T_2 returned to baseline for all renal layers: $T_2 = 44 \pm 3.8$ ms (CO), $T_2 = 53 \pm 5.6$ ms (OM), and $T_2 = 87 \pm 16.2$ ms (IM).

Figure 7 shows representative quantitative TVF maps obtained for baseline, transient pelvis and TPI, and recovery. A good qualitative correspondence was observed between the TVF maps and the T_2 maps. TVF maps showed clear changes of TVF following TPI. Figure 7 also shows the time course of changes in TVF in response to the TPI intervention for the first ($n = 3$) and second ($n = 4$) subgroups. During baseline for TVF, a mean value of 18.3 ± 2.5% (CO) and 28.1 ± 4.9% (OM) was observed. Following TPI, TVF_{cortex} increased by 6.8% and 3.4% for the first and second subgroups, respectively, and returned to baseline levels during the recovery phase, following cessation of TPI. A similar effect was observed in the OM: Following TPI, its TVF increased by 5.6% and 3.7% for first and second subgroups, again returning to baseline levels during the recovery phase. A different effect was observed in the IM: Following TPI, its TVF decreased by 12.2% and 16.4% for the first and second subgroups, and TVF returned to baseline levels during recovery.

To account for the different numbers of scans in the two subgroups, we took the mean of the TVF for all $n = 7$ rats during the baseline and intervention phases for statistical analysis. In response to the TPI intervention, significant changes in the TVF were observed in the CO ($p = 0.0003$),

TABLE 1 Representative tubular volume fraction (TVF) calculated after analyzing the T_2 decay of the synthetic data with bi-exponential analysis for a variety of TVF using different T_{2_long} as a fixed value for fitting. Simulation was performed for the in vivo protocol (first TE = 6.4 ms, interecho time ΔTE = 6.4, number of echoes = 13, $\alpha_{\text{refocusing pulse}} = 180°$, $T_{2\_long} = 500$ ms, $T_{2\_short} = 50$ ms, SNR = 30)

Ground truth		Underestimation				Right estimation		Overestimation			
T_{2_long} = 500 ms	Δ	T_{2_long} = 300 ms	Δ	T_{2_long} = 400 ms	Δ	T_{2_long} = 500 ms	Δ	T_{2_long} = 600 ms	Δ	T_{2_long} = 700 ms	Δ
0		5.7		5.3		5.1		5.0		4.9	
5.0	5.0	7.8	2.1	7.0	1.7	6.5	1.4	6.3	1.3	6.0	1.1
10.0	5.0	11.8	4.0	10.5	3.5	9.9	3.4	9.5	3.2	9.1	3.1
15.0	5.0	16.3	4.5	14.6	4.1	13.6	3.7	13.0	3.5	12.5	3.4
20.0	5.0	21.1	4.8	18.9	4.3	17.6	4.0	16.9	3.9	16.2	3.7
25.0	5.0	26.1	5.0	23.3	4.4	21.7	4.1	20.8	3.9	19.9	3.7
30.0	5.0	31.2	5.1	27.8	4.5	25.8	4.1	24.8	4.0	23.7	3.8
35.0	5.0	36.3	5.1	32.3	4.5	30.1	4.3	28.8	4.0	27.5	3.8
40.0	5.0	41.8	5.5	37.2	4.9	34.6	4.5	33.1	4.3	31.6	4.1
45.0	5.0	47.7	5.9	42.5	5.3	39.4	4.8	37.7	4.6	36.1	4.5
50.0	5.0	53.7	6.0	47.8	5.3	44.4	5.0	42.4	4.7	40.6	4.5
55.0	5.0	59.6	5.9	53.2	5.4	49.4	5.0	47.3	4.9	45.2	4.6
60.0	5.0	65.5	5.9	58.7	5.5	54.6	5.2	52.2	4.9	50.0	4.8
65.0	5.0	71.5	6.0	64.2	5.5	59.8	5.2	57.2	5.0	54.8	4.8
70.0	5.0	77.4	5.9	69.7	5.5	65.0	5.2	62.3	5.1	59.6	4.8
75.0	5.0	83.4	6.0	75.2	5.5	70.3	5.3	67.4	5.1	64.6	5.0
80.0	5.0	89.7	6.3	80.8	5.6	75.6	5.3	72.6	5.2	69.6	5.0
85.0	5.0	95.2	5.5	86.6	5.8	81.0	5.4	77.8	5.2	74.6	5.0
90.0	5.0	98.4	3.2	92.4	5.8	86.6	5.6	83.1	5.3	79.8	5.2
95.0	5.0	99.7	1.3	96.7	4.3	92.2	5.6	88.7	5.6	85.0	5.2
Mean average error for relative changes (Δ) =			1.01		0.74		0.71		0.75		0.83

Note: Relative changes (Δ) refer to differentiation of each TVF to the upper cell (increment of TVF). This table is intended to show what will happen if T_{2_long} is misestimated during the fitting process. Numbers are presented as percentages.

the OM ($p = 0.0207$), and the IM ($p = 0.0162$) (Figure 8). Pair-wise comparisons confirmed that, within the CO, the TVF increased significantly from baseline levels during the intervention ($p = 0.0005$) and decreased significantly during recovery ($p = 0.0325$); TVF values during the recovery phase were not significantly different from baseline levels ($p = 0.1814$; Figure 8). In the OM, pair-wise comparisons showed a significant increase in TVF between baseline and the intervention ($p = 0.0162$). The difference between intervention and recovery was also significant ($p = 0.0162$). Finally, the IM pair-wise comparison showed a significant reduction in TVF between baseline and intervention ($p = 0.0075$), which increased during recovery ($p = 0.0325$) to levels that were not significantly different from baseline ($p = 0.5930$; Figure 8). The R^2 values indicated a good fit for all in vivo TVF estimations, with the smallest R^2 value being 0.991.

4 | DISCUSSION

This is the first report on in vivo assessment of relative changes in the renal tubular volume fraction as a (patho)physiological metric. We demonstrate the feasibility of dynamic parametric mapping of the MRI relaxation time T_2 as a surrogate for TVF cartography and for monitoring physiological changes in the TVF. For the first time, we present parametric maps of TVF obtained under normal conditions and following increased pelvis and tubule pressure—a clinically relevant intervention. We

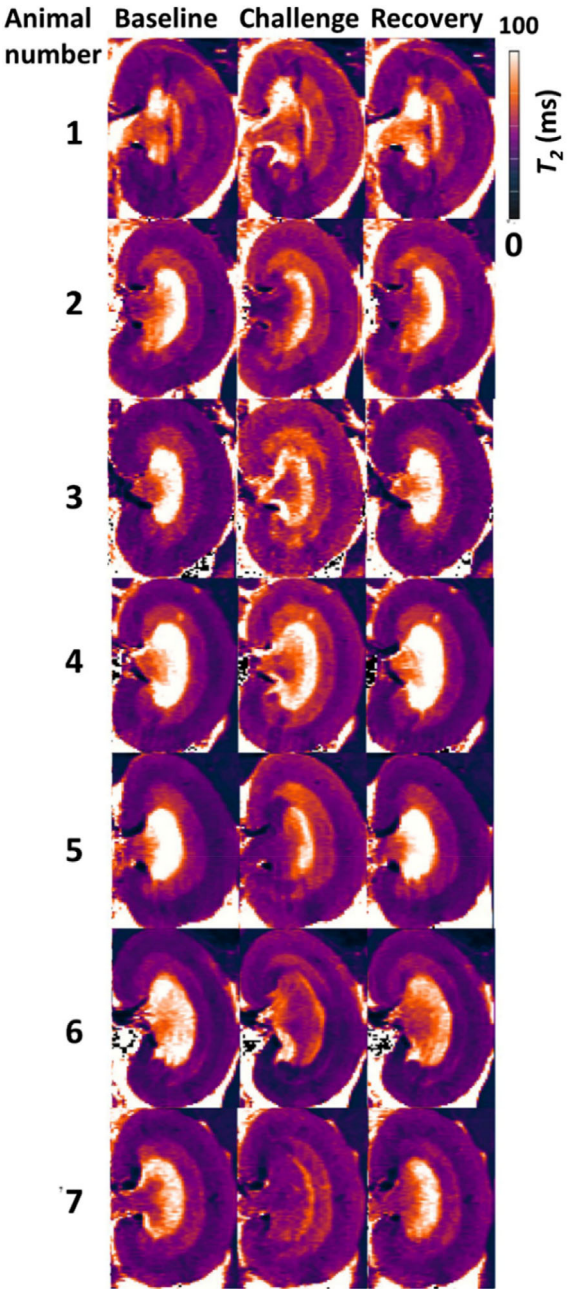

FIGURE 6 T_2 maps obtained from a mono-exponential fit for seven in vivo rat kidneys: baseline (*left*), during the intervention (*center*), and recovery (*right*). Substantial changes in T_2 during pelvis/ureter pressure increase are visually apparent. During baseline, we observed T_2 relaxation times (mean ± SD) of $T_2 = 44 \pm 3.6$ ms (cortex), $T_2 = 54 \pm 5.2$ ms (outer medulla), and $T_2 = 88 \pm 16$ ms (inner medulla). Following renal pelvis/tubular pressure increase, T_2 increasing was detected in the kidney for cortex (CO) and outer medulla (OM), and T_2 shortening for inner medulla (IM). An average T_2 of 49 ± 4.3 ms (CO), 57 ± 6.3 ms (OM) and 63 ± 11.4 ms (IM) was observed. Following release of pelvis and tubule pressure, T_2 returned to baseline for all renal layers. Possible artifacts are induced by combined pO_2/Laser-Flux probes, distorted kidney boundaries, air cavities, or fat-induced artifacts.

developed an MRI protocol tailored for T_2 mapping of the rat kidney and determined a suitable numerical solution for multi-exponential decomposition of the T_2 decay based on literature and numerical algorithms. Because in vivo experiments are always limited by the constraints of acquisition time, spatial resolution and SNR, we evaluated the multi-exponential decomposition approach in simulations using a broad range of conditions of T_2 mapping. This demonstrated the effect of image SNR and the long component fraction on the accuracy of TVF measurements. The simulations also highlighted how the flip angle and inter-TE in multi-echo spin-echo MRI affect the TVF assessment error. Validation in phantom experiments revealed a high accuracy (MAE < 1%) for the low-MAE T_2 mapping protocol. The accelerated T_2 mapping protocol customized for the in vivo study averaged over a variety of fractions ensured an average accuracy of MAE < 3%. Similarly, the phantom results demonstrated higher accuracy for smaller TVFs (MAE < 2%). The accuracy decreases for higher fractions of the long component. This means the TVF measurements for the CO are more accurate than for the OM and IM if the protocol is suboptimal.

Evaluation and validation of this approach in the phantom was followed by a proof-of-principle demonstration using data from an in vivo experiment. For this purpose, we applied a (patho-)physiologically relevant intervention, transiently increasing the pressure in the renal pelvis and tubules, while the rats were in the MRI scanner. The intervention induced significant changes in TVF in all three renal compartments. TVF increased significantly in CO and OM, and restored to baseline level when the TPI intervention was terminated. However, contrary to our expectations, we observed a significant decrease in TVF within the IM during the intervention, which returned to baseline levels during recovery. This finding contradicted our hypothesis that TPI would increase TVF in all renal layers. Following closer examination of the dynamic T_2 mapping data obtained during baseline, TPI and recovery, we noted an expansion of the renal pelvis during the intervention. The increase in intrapelvic pressure following the intervention was powerful enough to stretch the rather rigid tissue wall of the pelvis and was most likely compressing the comparatively softer tissue (including the tubules) of the portion of the IM that is enveloped by the pelvis.[51] This finding highlights the potential of our approach to offer insights into biomechanical interactions between different layers of kidney, which could have physiological implications.

In this work, our MRI-based monitoring was focused on retrospective assessment of changes in TVF during an acute pathophysiological scenario. Future steps will include prospective and real-time application of T_2 decomposition and TVF measurement, integrating our

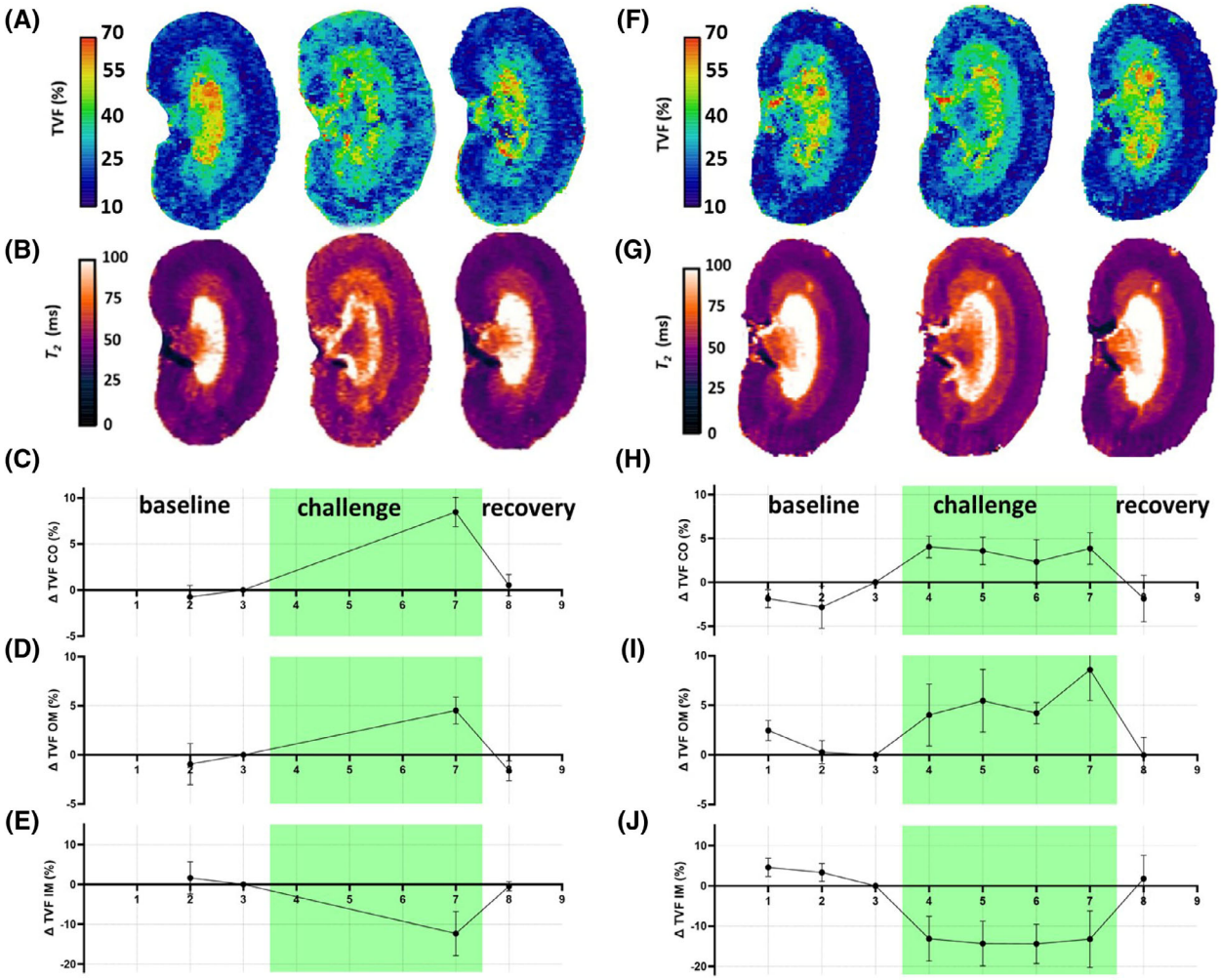

FIGURE 7 Time courses during renal pelvis/tubular pressure increase. A,B, Exemplary tubular volume fraction (TVF) and T_2 maps (mono-exponential fit) obtained for a rat kidney in vivo of the first subgroup ($n = 3$). Time course of the TVF changes (mean ± SEM) for cortex (C; CO), outer medulla (D; OM), and inner medulla (E; IM) before the intervention (*baseline*), during the intervention (*green area*), and during recovery acquired for the first subgroup ($n = 3$). F–J, Time courses during renal pelvis/tubular pressure increase, obtained for the second subgroup ($n = 4$). F,G, Exemplary TVF and T_2 maps (mono-exponential fit) obtained for a rat kidney in vivo. Time course of the TVF changes (mean ± SEM) for CO (H), OM (I), and IM (J) before the intervention (*baseline*), during the intervention (*green area*), and during recovery acquired for the second subgroup ($n = 4$).

decomposition analysis directly into the image reconstruction and postprocessing pipeline of the MR scanner. The TVF computation time for each fit was 90 ms, which is in compliance with dynamic renal T_2 mapping that commonly uses a temporal resolution of 10–90 s per map, and hence is suitable for on-the-fly assessment of TVF. This would benefit inclusion of TVF cartography into multiparametric MRI protocols of the kidney. It would also support extraction of radiomic features from the kidney by including a physiological metric into the multivariate analysis of renal MRI data.

To complement preclinical animal studies en route to clinical translation, our approach to MRI-based TVF could be applied to renal organoids. Organoids are 3D multicellular cultures that resemble the structure and physiology of their organ of origin. Recent reports have described protocols for generating 3D kidney tubule organoids—tubuloids—from a human tissue,[52,53] which could support studies of kidney physiology, disease modeling, high-throughput drug screening, and regenerative medicine.[54] Our approach to TVF monitoring provides an imaging methodology that can facilitate studies in organoids, which would be in full alignment with the 3R principles on the use of animal models.

Simulation of T_2 decay curves for a broad range of physical and experimental conditions provides a comprehensive library of TVF fingerprints.[55] Benchmarking experimentally acquired T_2 decays against this library could reduce time-consuming postprocessing and fitting. Combining our approach with deep learning algorithms,

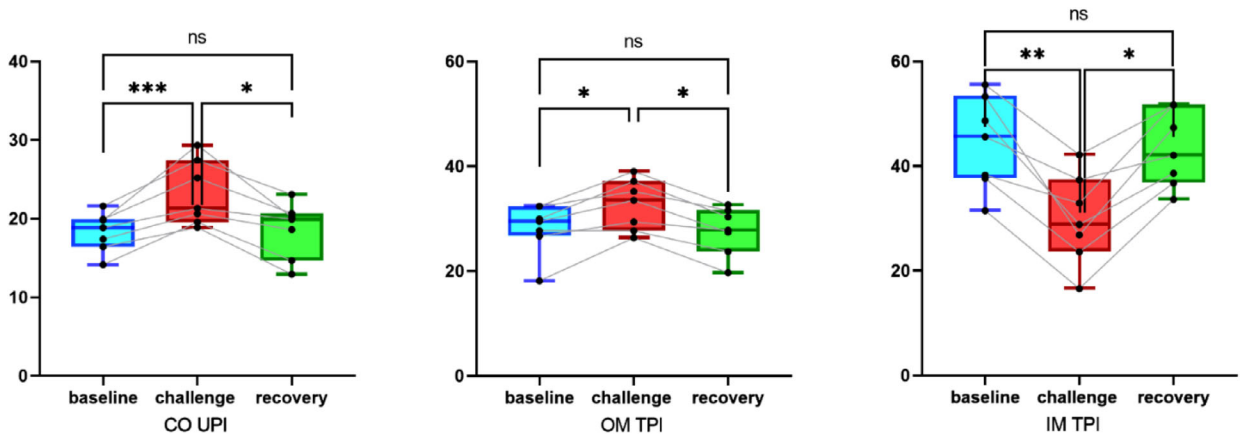

FIGURE 8 Box-and-whisker plots showing changes of tubular volume fraction (TVF) during pelvis/ureter pressure increase. TVF was significantly increased in the kidneys' cortex and outer medulla during intervention ($p = 0.0005/p = 0.0162$; Dunn's multiple test vs. baseline). TVF reduction was significant for inner medulla ($p = 0.0075$; Dunn's multiple test vs. baseline). The box-and-whisker plots display the first and third quartiles, with the line within the box representing the median value. The whiskers denote the minimum and maximum values. Volumes were examined by non-parametric multicomparison, comparing TVF among all three conditions using Dunn's multiple test for multiple comparisons ($n = 7$ subjects).

the reliability and speed of such T_2 fitting could be further enhanced. This would also benefit studies aiming to decode the links between TVF as a mesoscopic marker, and data from histopathological, physiological, and functional measurements. Ultimately, this would help understand renal disease determinants, even in cases in which TVF changes are subtle, such as in polycystic kidney disease or severe fibrosis. However, developing deep learning algorithms and neural networks relies on having a large data set with accurate training data that cover biological variability and pathophysiological conditions.

Because changes in the TVF likely induce alterations in the renal blood volume fraction, they will result in changes in renal T_2* independent of changes in blood oxygenation. Indeed, the TVF is a confounding factor influencing the relationship between renal T_2*, oxygen saturation of hemoglobin, and tissue oxygen tension.[45,56] Hence, T_2 assessments of changes in the TVF are highly relevant for elucidating the mechanisms of renal pathophysiology and will help to accurately determine the pathophysiological role of changes in renal oxygenation assessed by renal T_2* mapping.

Previous ex vivo TVF examinations of the renal cortex reported $TVF_{cortex,ex\_vivo} = 23 \pm 2\%$ under control conditions and $TVF_{cortex\_ex\_vivo} = 31 \pm 4\%$ for acute ischemic injury to a solitary kidney.[2] Although this is in accordance with our findings, future in vivo validation of our MRI approach to TVF assessment with intravital microscopy (i.e. for quantitative comparison of changes in the vascular and renal tubular compartments with those observed by T_2* and T_2) is warranted.

In conclusion, our investigations have the potential to help uncover the mechanisms leading to acute kidney injury and progression to chronic kidney disease. Monitoring of relative changes in renal TVF in vivo using dynamic parametric MRI provides a potential rapid, noninvasive marker for kidney disease.[57] This approach will be invaluable for gaining a better mechanistic understanding of renal (patho-)physiology.

ACKNOWLEDGMENTS

This work was funded in part by the German Research Foundation (394046635, SFB 1365, and RENOPROTECTION, to Thoralf Niendorf, Erdmann Seeliger, Sonia Waiczies, Thomas Gladytz, and Kathleen Cantow). The authors thank A. Pohlmann (Max-Delbrueck Center for Molecular Medicine in the Helmholtz Association, Berlin, Germany), and A. Anger, and B. Flemming (Institute of Translational Physiology, Charité–Universitätsmedizin, Berlin, Germany) for technical and other support. Open Access funding enabled and organized by Projekt DEAL.

DATA AVAILABILITY STATEMENT

The imaging data acquired for in vivo experiments (section 2.4/3.3) are openly available at OSF under https://osf.io/8epbt.

ORCID

Ehsan Tasbihi https://orcid.org/0000-0002-4190-7202
Ludger Starke https://orcid.org/0000-0002-0359-0101
Sonia Waiczies https://orcid.org/0000-0002-9916-9572

REFERENCES

1. Knepper MA, Danielson RA, Saidel GM, Post RS. Quantitative analysis of renal medullary anatomy in rats and rabbits. *Kidney Int.* 1977;12:313-323. doi:10.1038/ki.1977.118

2. Pagtalunan ME, Olson JL, Tilney NL, Meyer TW. Late consequences of acute ischemic injury to a solitary kidney. *J Am Soc Nephrol.* 1999;10:366-373. doi:10.1681/ASN.V102366
3. Anders H-J, Kitching AR, Leung N, Romagnani P. Glomerulonephritis: immunopathogenesis and immunotherapy. *Nat Rev Immunol.* 2023;23:453-471. doi:10.1038/s41577-022-00816-y
4. Cao J, Zhu S, Ye M, et al. Comparison of renal artery vs renal artery-vein clamping during partial nephrectomy: a system review and meta-analysis. *J Endourol.* 2020;34:523-530. doi:10.1089/end.2019.0580
5. Chadban SJ, Atkins RC. Glomerulonephritis. *Lancet*. 2005;365:1797-1806.
6. Haase M, Bellomo R, Story D, et al. Effect of mean arterial pressure, haemoglobin and blood transfusion during cardiopulmonary bypass on post-operative acute kidney injury. *Nephrol Dial Transplant.* 2012;27:153-160. doi:10.1093/ndt/gfr275
7. Jongkind V, Yeung KK, Akkersdijk GJ, et al. Juxtarenal aortic aneurysm repair. *J Vasc Surg.* 2010;52:760-767. doi:10.1016/j.jvs.2010.01.049
8. Kellum JA, Prowle JR. Paradigms of acute kidney injury in the intensive care setting. *Nat Rev Nephrol.* 2018;14:217-230. doi:10.1038/nrneph.2017.184
9. Tonneijck L, Muskiet MH, Smits MM, et al. Glomerular hyperfiltration in diabetes: mechanisms, clinical significance, and treatment. *J Am Soc Nephrol.* 2017;28:1023-1039. doi:10.1681/ASN.2016060666
10. Roumelioti M-E, Ing TS, Rondon-Berrios H, et al. Principles of quantitative water and electrolyte replacement of losses from osmotic diuresis. *Int Urol Nephrol.* 2018;50:1263-1270. doi:10.1007/s11255-018-1822-0
11. Fähling M, Seeliger E, Patzak A, Persson PB. Understanding and preventing contrast-induced acute kidney injury. *Nat Rev Nephrol.* 2017;13:169-180. doi:10.1038/nrneph.2016.196
12. Seeliger E, Sendeski M, Rihal CS, Persson PB. Contrast-induced kidney injury: mechanisms, risk factors, and prevention. *Eur Heart J.* 2012;33:2007-2015. doi:10.1093/eurheartj/ehr494
13. Chung KJ, Kim JH, Min GE, et al. Changing trends in the treatment of nephrolithiasis in the real world. *J Am Soc Nephrol.* 2019;33:248-253. doi:10.1089/end.2018.0667
14. Huang S-W, Tsai C-Y, Tseng C-S, et al. Comparative efficacy and safety of new surgical treatments for benign prostatic hyperplasia: systematic review and network meta-analysis. *BMJ*. 2019;367:l5919. doi:10.1136/bmj.l5919
15. Preminger GM. *Urinary Tract Obstruction*. Duke Comprehensive Kidney Stone Center; 2022. Accessed January 23, 2024. https://www.msdmanuals.com/professional/genitourinary-disorders/obstructive-uropathy/obstructive-uropathy#v6666078
16. Tokas T, Herrmann TR, Skolarikos A, et al. Pressure matters: intrarenal pressures during normal and pathological conditions, and impact of increased values to renal physiology. *World J Urol.* 2019;37:125-131. doi:10.1007/s00345-018-2378-4
17. Le Bihan D, Breton E, Lallemand D, Aubin M-L, Vignaud J, Laval-Jeantet M. Separation of diffusion and perfusion in intravoxel incoherent motion MR imaging. *Radiology.* 1988;168:497-505. doi:10.1148/radiology.168.2.3393671
18. Periquito JS, Gladytz T, Millward JM, et al. Continuous diffusion spectrum computation for diffusion-weighted magnetic resonance imaging of the kidney tubule system. *Quant Imag Med Su*. 2021;11:3098-3119. doi:10.21037/qims-20-1360
19. Reed GD, von Morze C, Verkman AS, et al. Imaging renal urea handling in rats at millimeter resolution using hyperpolarized magnetic resonance relaxometry. *Tomography.* 2016;2:125-137. doi:10.18383/j.tom.2016.00127
20. Zhao WT, Herrmann KH, Sibgatulin R, et al. Perfusion and T2 relaxation time as predictors of severity and outcome in sepsis-associated acute kidney injury: a preclinical MRI study. *JMRI.* 2023;58:1954-1963. doi:10.1002/jmri.28698
21. Pohlmann A, Hentschel J, Fechner M, et al. High temporal resolution parametric MRI monitoring of the initial ischemia/reperfusion phase in experimental acute kidney injury. *PloS One.* 2013;8:e57411. doi:10.1371/journal.pone.0057411
22. Lee SP, Silva AC, Ugurbil K, Kim SG. Diffusion-weighted spin-echo fMRI at 9.4 T: microvascular/tissue contribution to BOLD signal changes. *Magn Reson Med.* 1999;42:919-928. doi:10.1002/(sici)1522-2594(199911)42:5<919::aid-mrm12>3.0.co;2-8
23. Gladytz T, Millward JM, Cantow K, et al. Reliable kidney size determination by magnetic resonance imaging in pathophysiological settings. *Acta Physiol.* 2021;233:e13701. doi:10.1111/apha.13701
24. Sobol W, Pintar M. NMR spectroscopy of heterogeneous solid-liquid mixtures. Spin grouping and exchange analysis of proton spin relaxation in a tissue. *Magn Reson Med.* 1987;4:537-554. doi:10.1002/mrm.1910040605
25. Tasbihi E, Gladytz T, Starke L, Millward JM, Seeliger E, Niendorf T. Toward assessment of renal tubule volume fraction in rat kidney using decomposition of parametric T2 mapping. In: *Proceedings of the 32nd Annual Meeting of ISMRM*, Toronto, Ontario, Canada. 2023. Digital poster 4441
26. Mulkern R, Bleier A, Adzamli I, Spencer R, Sandor T, Jolesz F. Two-site exchange revisited: a new method for extracting exchange parameters in biological systems. *Biophys J.* 1989;55:221-232. doi:10.1016/S0006-3495(89)82797-3
27. Vasilescu V, Katona E, Simplaceanu V, Demco D. Water compartments in the myelinated nerve. III. Pulsed NMR result. *Experientia*. 1978;34:1443-1444. doi:10.1007/BF01932339
28. Yoshimura S, Tanaka H, Kawabata S, et al. Effect of urinary glucose concentration and pH on signal intensity in magnetic resonance images. *Jpn J Radiol.* 2022;40:930-938. doi:10.1007/s11604-022-01273-2
29. Chenxi Hu, Reeves SJ. Trust Region Methods for the Estimation of a Complex Exponential Decay Model in MRI With a Single-Shot or Multi-Shot Trajectory. *IEEE Trans Image Process*, 2015;24:3694–3706. doi: 10.1109/tip.2015.2442917
30. Jamarik J, Vojtisek L, Schwarz D. Uncovering cortical layers with multi-exponential analysis: a region of interest study. 2022 30th European Signal Processing Conference. 1353–1356. doi: 10.23919/eusipco55093.2022.9909806
31. Yuan YX. A Review of Trust Region Algorithms for Optimization. ICM99: Proceedings of the Fourth International Congress on Industrial and Applied Mathematics. 271-282.
32. Hennig J. Multiecho imaging sequences with low refocusing flip angles. *JMR.* 1988;78:397-407.
33. Hennig J. Echoes—how to generate, recognize, use or avoid them in MR-imaging sequences. Part I: Fundamental and not so fundamental properties of spin echoes. *Concepts Magn Reson.* 1991;3:125-143. doi:10.1002/CMR.1820030302

34. Mehdizadeh N, Wilman AH. Myelin water fraction mapping from multiple echo spin echoes and an independent B1+ map. *Magn Reson Med.* 2022;88:1380-1390. doi:10.1002/mrm.29286
35. Prasloski T, Mädler B, Xiang QS, MacKay A, Jones C. Applications of stimulated echo correction to multicomponent T2 analysis. *Magn Reson Med.* 2012;67:1803-1814. doi:10.1002/mrm.23157
36. Periquito JS, Starke L, Santos CM, et al. Analysis protocols for MRI mapping of the blood oxygenation-sensitive parameters T(2)* and T(2) in the kidney. *Methods Mol Biol.* 2021;2216:591-610. doi:10.1007/978-1-0716-0978-1_36
37. Price RR, Axel L, Morgan T, et al. Quality assurance methods and phantoms for magnetic resonance imaging: report of AAPM nuclear magnetic resonance task group No. 1. *Med Phys.* 1990;17:287-295. doi:10.1118/1.596566
38. Cantow K, Gladytz T, Millward JM, Waiczies S, Niendorf T, Seeliger E. Monitoring kidney size to interpret MRI-based assessment of renal oxygenation in acute pathophysiological scenarios. *Acta Physiol.* 2023;237:e13868. doi:10.1111/apha.13868
39. Cantow K, Ladwig-Wiegard M, Flemming B, Pohlmann A, Niendorf T, Seeliger E. Monitoring renal hemodynamics and oxygenation by invasive probes: experimental protocol. Preclinical MRI of the Kidney: Methods and Protocols. Humana Press; 2021:327-347. doi:10.1007/978-1-0716-0978-1_19
40. Grosenick D, Cantow K, Arakelyan K, Wabnitz H, Flemming B, Skalweit A. Detailing renal hemodynamics and oxygenation in rats by a combined near-infrared spectroscopy and invasive probe approach. *Biomed Opt Express*. 2015;6:309-323. doi:10.1364/BOE.6.000309
41. Kaucsar T, Hosszu A, Seeliger E, Reimann HM, Fekete A. Preparation and monitoring of small animals in renal MRI. *Methods Mol Biol.* 2021;2216:45-55. doi:10.1007/978-1-0716-0978-1_3
42. Seeliger E, Cantow K, Arakelyan K, Ladwig M, Persson PB, Flemming B. Low-dose nitrite alleviates early effects of an X-ray contrast medium on renal hemodynamics and oxygenation in rats. *Invest Radiol.* 2014;49:70-77. doi:10.1097/RLI.0b013e3182a6fea6
43. Gottschalk CW, Mylle M. Micropuncture study of pressures in proximal tubules and peritubular capillaries of the rat kidney and their relation to ureteral and renal venous pressures. *Am J Physiol.* 1956;185:430-439. doi:10.1152/ajplegacy.1956.185.2.430
44. Pohlmann A, Arakelyan K, Hentschel J, et al. Detailing the relation between renal T2* and renal tissue pO2 using an integrated approach of parametric magnetic resonance imaging and invasive physiological measurements. *Invest Radiol.* 2014;49:547-560. doi:10.1097/RLI.0000000000000054
45. Pohlmann A, Cantow K, Hentschel J, et al. Linking non-invasive parametric MRI with invasive physiological measurements (MR-PHYSIOL): towards a hybrid and integrated approach for investigation of acute kidney injury in rats. *Acta Physiol.* 2013;207:673-689. doi:10.1111/apha.12065
46. Riazy L, Milani B, Periquito JS, et al. Subsegmentation of the kidney in experimental MR images using morphology-based regions-of-interest or multiple-layer concentric objects. *Methods Mol Biol.* 2021;2216:549-564. doi:10.1007/978-1-0716-0978-1_33
47. Søgaard SB, Andersen SB, Taghavi I, et al. Super-resolution ultrasound imaging provides quantification of the renal cortical and medullary vasculature in obese zucker rats: a pilot study. *Diagnostics.* 2022;12:1626. doi:10.3390/diagnostics12071626
48. Kassambara A. rstatix: Pipe-friendly framework for basic statistical tests (R package Version 0.7. 0) [Computer software]. 2021.
49. Morgan-Wall T. rayshader: Create Maps and Visualize Data in 2D and 3D. 2020. Accessed January 5, 2024. https://github.com/tylermorganwall/rayshader
50. Dinno A, Dinno MA. Package 'dunn. test'. *CRAN Rep.* 2017;10:1-7.
51. Vroomen LG, John NT, Fuijmori M, Sivaraman A, Felsen D, Srimathveeravalli G. A new intrasurgical technique to safely and reproducibly induce partial unilateral urinary obstruction and renal scarring in a rat model. *Int Urol Nephrol.* 2020;52:1209-1218. doi:10.1007/s11255-020-02421-1
52. Guo H, Deng N, Dou L, et al. 3-D human renal tubular organoids generated from urine-derived stem cells for nephrotoxicity screening. *ACS Biomater Sci Eng.* 2020;6:6701-6709. doi:10.1021/acsbiomaterials.0c01468
53. Schutgens F, Rookmaaker MB, Margaritis T, et al. Tubuloids derived from human adult kidney and urine for personalized disease modeling. *Nat Biotechnol.* 2019;37:303-313. doi:10.1038/s41587-019-0048-8
54. Yousef Yengej FA, Jansen J, Rookmaaker MB, Verhaar MC, Clevers H. Kidney organoids and tubuloids. *Cells.* 2020;9:1326. doi:10.3390/cells9061326
55. Shpringer G, Bendahan D, Ben-Eliezer N. Accelerated reconstruction of dictionary-based T2 relaxation maps based on dictionary compression and gradient descent search algorithms. *Magn Reson Med.* 2022;87:56-66. doi:10.1016/j.mri.2021.12.006
56. Niendorf T, Pohlmann A, Arakelyan K, et al. How BOLD is blood oxygenation level-dependent (BOLD) magnetic resonance imaging of the kidney? Opportunities, challenges and future directions. *Acta Physiol.* 2015;213:19-38. doi:10.1111/apha.12393
57. Chávez-Iñiguez JS, Navarro-Gallardo GJ, Medina-González R, Alcantar-Vallin L, García-García G. Acute kidney injury caused by obstructive nephropathy. *Int J Nephrol.* 2020;2020:1-10. doi:10.1155/2020/8846622

How to cite this article: Tasbihi E, Gladytz T, Millward JM, et al. In vivo monitoring of renal tubule volume fraction using dynamic parametric MRI. *Magn Reson Med*. 2024;1-14. doi: 10.1002/mrm.30023